A teleoperated control approach for anthropomorphic manipulator using magneto-inertial sensors

A. Noccaro[1], **F. Cordella**[2], **L. Zollo**[2], **G. Di Pino**[1], **E. Guglielmelli**[2], and **D. Formica**[3]

[1]Unit of Neurophysiology and Neuroengineering of Human-Technology Interaction, Department of Medicine, Università Campus Bio-Medico, via Alvaro del Portillo 21, 00128, Rome, Italy

[2]Unit of Biomedical Robotics and Biomicrosystems, Department of Engineering, Università Campus Bio-Medico, via Alvaro del Portillo 21, 00128, Rome, Italy

[3]Unit of Biomedical Robotics and Biomicrosystems, Department of Engineering and with the Unit of Neurophysiology and Neuroengineering of Human-Technology Interaction, Department of Medicine, Università Campus Bio-Medico di Roma, via Alvaro del Portillo 21, 00128, Rome, Italy

Abstract

In this paper we propose and validate a teleoperated control approach for an anthropomorphic redundant robotic manipulator, using magneto-inertial sensors (IMUs). The proposed method allows mapping the motion of the human arm (used as the master) on the robot end-effector (the slave). We record arm movements using IMU sensors, and calculate human forward kinematics to be mapped on robot movements. In order to solve robot kinematic redundancy, we implemented different algorithms for inverse kinematics that allows imposing anthropomorphism criteria on robot movements. The main objective is to let the user to control the robotic platform in an easy and intuitive manner by providing the control input freely moving his/her own arm and exploiting redundancy and anthropomorphism criteria in order to achieve human-like behaviour on the robot arm. Therefore, three inverse kinematics algorithms are implemented: Damped Least Squares (DLS), Elastic Potential (EP) and Augmented Jacobian (AJ). In order to evaluate the performance of the algorithms, four healthy subjects have been asked to control the motion of an anthropomorphic robot arm (i.e. the Kuka Light Weight Robot 4+) through four magneto-inertial sensors (i.e. Xsens Wireless Motion Tracking sensors - MTw) positioned on their arm. Anthropomorphism indices and position and orientation errors between the human hand pose and the robot end-effector pose were evaluated to assess the performance of our approach.

I   Introduction

Teleoperation was introduced for controlling robotic manipulators operating in hazardous environment [1]. Later, it was used in many other applications, such as robot-assisted surgery [2] and tele-rehabilitation [3]. A telerobotic system is basically composed of a master and a slave robot, with the slave usually controlled by a human operator through the master interface.

a.noccaro@unicampus.it.

Always more often, the slave exhibits anthropomorphic kinematic chain (and appearance). Indeed, the introduction of anthropomorphic criteria in robot design has several advantages: (i) safety improvements during human-robot interaction, since the human subjects can predict more easily human-like robot motion, (ii) higher robot acceptance from the human beings, (iii) more intuitive control from the user when his/her movements are mapped into movements of the slave side [4] [5] [6]. Furthermore, the redundancy of the anthropomorphic robots allows to achieve movements that are comparable to the one performed by the operator arm (that is a redundant manipulator from a kinematic viewpoint) [7].

The input provided by the human operator on the master side can be acquired by different devices, which are usually robots, joysticks or other systems, which in general have different kinematics, number of Degrees of Freedom (DoFs) and workspace with respect to the slave [1]. Therefore, the human operator typically needs a specific training to learn how to control the slave.

An alternative approach consists in using a motion tracking system for acquiring the human movements (such as cameras [8], magneto-inertial sensors (IMUs) [9]), and map them onto robot movements. In this case, the similarity between the human arm and the anthropomorphic robot in terms of kinematic chain, allows the user to control more easily and intuitively the robotic platform by means of free movements performed on the master side, thus not requiring particular skills or training to use the interface.

Once the master movements are acquired, they should be mapped into corresponding slave movements by means of an appropriate human to robot motion mapping approach. Several mapping strategies are proposed in the literature such as joint-to-joint, fingertip, functional pose and object-specific mapping [10] [11].

The fingertips mapping is the most adopted method in the literature since, unlike the other methods, it can be easily adapted to a wide range of systems even though it is conceived for hand motion mapping. It is based on the computation of forward kinematics for each human finger to obtain their positions in 3D space. Then the inverse kinematics for each robotic finger is computed, achieving the same 3D positions of the human one [12].

Most of the studies proposed in the literature adopted the fingertip method for mapping the motion of a human arm on robotic manipulators, focusing on achieving high accuracy in terms of end-effector pose, but without taking into account anthropomorphic criteria not allowing to achieve the same configuration for the human and the robot arm in the joint space [13].

Therefore, the main objective of this paper is to overcome this limitation by proposing a teleoperated control approach for an anthropomorphic robot manipulator that allows mapping the motion of the human hand on the robot end-effector by exploiting a fingertip mapping method and meeting anthropomorphic criteria in the joint space. Three different inverse kinematics algorithms (i.e. Damped Least Squares (DLS) [1], Elastic Potential (EP) [1] and Augmented Jacobian (AJ) [14]) are compared in order to find the best method for

control the robot arm [15] [16]. The EP and AJ methods basically exploit the robot redundancy in order to achieve anthropomorphic configurations of the kinematic chain.

It is interesting to note that the proposed teleoperated control can be intuitively and easily used by the subjects since the human motion tracking on the master side is achieved by means of magneto-inertial sensors positioned on the subject arm. The user can control the robot arm by freely moving his/her own arm guaranteeing in this way a wide extended workspace. Furthermore, the setup time is low as well as the costs of the master system. This makes the system suitable for industrial environment so as for everyday life contexts, such as assistive or rehabilitation scenarios.

The proposed approach has been experimentally validated on the anthropomorphic robotic arm Kuka Light Weight Robot (LWR) 4+ [18], controlled by the user through four Xsens Wireless Motion Tracking sensors (MTw) [19]. An experimental study on four healthy subjects have been carried out in order to compare the performance of the three inverse kinematic algorithms. The recruited subjects were asked to control the robotic arm to reach three target poses in the robot workspace by using the three teleoperated controls. Position and orientation errors between human hand and robot end-effector were evaluated to assess task performances. Additionally for the EP and AJ approaches the position error between the human and the robot elbow joint was evaluated as anthropomorphism index.

The paper is organized as follows: Section II presents the adopted methodology, the experimental setup and describes the implemented algorithms. Section III focuses on the results. Finally, in Section IV conclusion and future works are discussed.

II Material and Methods

A Proposed approach

The proposed teleoperated control strategy is based on a forward-inverse kinematics approach for human to robot motion mapping. On the master side the human arm motion was acquired by a motion tracking system, which provides human arm forward kinematics (see Sect. II-C). Then, the inverse kinematics was computed for providing the robot joint angle values, achieving a robot end-effector pose equal to the one of the human hand (see Sect. II-D). Moreover, taking advantage of the robot redundancy, the initial configuration was selected in order to obtain a robot-human joint correspondence. On the slave side three different inverse kinematics algorithms were implemented and compared. In particular, elbow position data were processed in the EP and in the AJ methods in order to achieve human-like robot motion. Indeed, previous studies investigated the human motion, focusing on what anthropomorphism means and how it can be measured, expecially for replicating it on an arm-hand robotic system [15], [16], [17]. In the end, anthropomorphism and its measure have been defined through the comparison between human and robot motion. Many comparison criteria have been proposed and analyzed. Among them, the minimization of the distance between human and robot elbow joints resulted to be the best criterion for obtaining an anthropomorphic motion with the robotic system.

B Experimental Setup

On the slave side a 7 DoFs robotic arm (i.e. the KUKA LWR4+) was used as the anthropomorphic manipulator. It is an anthropomorphic robotic arm, which communicates with a remote PC through the Fast Research Interface (FRI) Library, provided by the manufacturer. On the master side four wireless Xsens Motion Trackers were positioned on the human body in order to acquire human arm motion. MTws are magneto-inertial units and make it possible to record orientation data thanks to a Kalman Filter [20].

The four MTws were placed on the human thorax, upper arm, forearm and hand, using click-in body straps included into the Xsens kit (Fig. 1).

Orientation data were wireless recorded connecting the sensors to the Awinda Station. The Station was also connected through USB to an Asus PC with Ubuntu 14.04 OS. The PC established an UDP protocol based communication with the robot, through an Ethernet cable.

Algorithms, both for recording MTws data and for controlling the robot, were implemented in C++ language.

The initial configuration of the human and robot arms was defined in order to obtain a robot-human joint correspondence. Hence, as shown in Figure 1, the robot second joint coincides with the human shoulder joint, the fourth robot joint coincides with the human elbow joint, etc. Notice that the KUKA end-effector corresponds to the human palm, in order to avoid wrist singularity. Afterwards, both robot and human frames were defined according to Denavit-Hartenberg representation.

C Forward Kinematics

Human links orientation data were recorded from MTws at 100 Hz as rotation matrices. Since the sensors were placed manually on the human arm, sensor frames turn out to be not aligned to the previously defined human frames. Therefore, a calibration procedure was executed in order to re-align these frames. The calibration provides the rotation matrix between each sensor frame and its related human link frame. The matrices are computed by processing accelerometer and gyroscope data acquired during human arm rotation around fixed axes (see [21] for details on the calibration procedure).

Afterwards, the human hand pose was computed. Assuming that the sensors were rigidly connected to the human links, each human joint position was computed as the product between the sensor frame axes aligned with the related link and the link length L_{link}. All measures were referred to the thorax reference frame R^{th0} at the time 0, with the operator in standing position (see Fig. 1).

Then, as shown in Fig. 1, the hand position p_{hand} was computed by means of a vectorial sum of human joint positions ($p_{shoulder}$, p_{elbow}, p_{wrist}), as in Eq. 1-4,

$$p_{shoulder}^{th0} = R_{th}^{th0} * v_{shoulder} \quad (1)$$

$$p_{elbow}^{th0} = p_{shoulder}^{th0} - R_{arm0}^{th0} * R_{arm}^{arm0} * v_{arm} \quad (2)$$

$$p_{wrist}^{th0} = p_{elbow}^{th0} - R_{for0}^{th0} * R_{for}^{for0} * v_{forearm} \quad (3)$$

$$p_{hand}^{th0} = p_{wrist}^{th0} - R_{hand0}^{th0} * R_{hand}^{hand0} * v_{hand} \quad (4)$$

with $v_{shoulder} = [0 \quad L_{shoulder} \quad 0]^T$, $v_{arm} = [L_{arm} \quad 0 \quad 0]^T$, $v_{for} = [L_{forearm} \quad 0 \quad 0]^T$ and $v_{hand} = [0 \quad 0 \quad L_{hand}]^T$.

R^{link0} represents each link reference frame at the starting time 0 (see Fig. 1). The hand orientation was basically provided by the orientation of the corresponding sensor.

$$R_{hand}^{th0} = R_{hand0}^{th0} * R_{hand}^{hand0} \quad (5)$$

It is worth noticing that the robot link lengths were used in liue of the human one (i.e. L_{link} in Eq. 1-4), thanks to the initial configuration previously defined (Fig. 1) [15].

Initially, the hand pose was referred to the thorax frame. Then, it was computed with respect to the KUKA base frame, taking into account also the rotation between the robot end-effector and the human hand frames.

$$p_{hand}^{BK} = R_{th0}^{BK} * p_{hand}^{th0} \quad (6)$$

$$R_{hand}^{BK} = R_{th0}^{BK} * R_{hand}^{th0} * R_{7K}^{hand} \quad (7)$$

Therefore, starting from the human hand pose referred to the thorax frame, the corresponding robot end effector pose with respect to the robot base frame was obtained.

D   Inverse Kinematics

In order to control the robot in the joint space taking advantage of the robot redundancy, three inverse kinematic algorithms were implemented and compared.

The DLS algorithm reduces the mean joint velocities, accepting a higher error near singular configurations. The inverse of Jacobian is replaced by a damped least squares expression (Eq. 8 and 9),

$$q(t_{k+1}) = q(t_k) + J^{DLS}(q(t_k)) * (v + Ke) * (t_{k+1} - t_k) \quad (8)$$

$$J^{DLS} = J^T(JJ^T + k^2 I)^{-1} \quad (9)$$

where $q(t_{k+1})$ represents the robot joint angles vector for a $k+1$ time sample, J is the robot Jacobian, v is the desired speed in cartesian space, K is a positive squared matrix, e represents the error between the desired and the actual pose in cartesian space, k is a damping constant and I is the identity matrix.

In the EP algorithm, the null projector is used to minimize a cost function w. For our application, this function is chosen to be an elastic potential, that represents a virtual spring connecting robot and human elbows, in order to minimize their distances. The algorithm expression is

$$q(t_{k+1}) = q(t_k) + (J*(q(t_k)) * Ke - (I_n - J*J)\dot{q}_0) * (t_{k+1} - t_k) \quad (10)$$

$$J* = J^T(JJ^T)^{-1} \quad (11)$$

where I_n is a squared identity matrix of nxn dimension.

$$\dot{q}_0 = k_0\left(\frac{\delta w(q)}{\delta q}\right)^T \quad ; \quad w = k_{elastic}\left(\|p_{he} - p_{re}\|\right)^2 \quad (12)$$

If the robot elbow position p_{re} is the same of the human one p_{he}, the spring is at rest position, on the contrary the more is the distance between the joints, the more the spring is strained and the elastic potential is high. At the beginning, a symbolic expression of the null projector (elastic potential derivative) was computed. Then, numerical solutions were calculated for each forward kinematics output according to Equations 10 and 11.

Since the forward kinematics evaluates the desired pose at a frequency of 100 Hz, the inverse kinematics output was computed at the same frequency. Each algorithm loop was computed N times before providing output, assuming $N * t_{IK} \le \frac{1}{100}$, with t_{IK} representing the algorithm computational time. This approach was adopted for all the three algorithms. The AJ algorithm was implemented using the swivel angle as elbow position measure [14]. This angle a represents the elbow position for fixed shoulder and hand positions (see Fig. 2).

The Augmented Jacobian J_A is computed adding to the Jacobian a row which represents the relation between the time derivative of a and the joints configuration. Also the cartesian pose (and the related v and e values) is augmented with the additional swivel angle value.

$$q(t_{k+1}) = q(t_k) + \left(J_A^{-1} q(t_k) * (v + Ke)\right) * (t_{k+1} - t_k) \quad (13)$$

$$J_A^{DLS} = J_A^T \left(J_A J_A^T + k^2 I_n\right)^{-1} \quad (14)$$

The algorithm was implemented according to Eq. 13 and 14, where I_n is the nxn identity matrix and J_A^{-1} is replaced by J_A^{DLS} in order to avoid singularity.

E Experimental Protocol

Four healthy subjects, 25.4 ± 1.6 years old, volunteered to participate in the study. They were asked to use the IMU sensors positioned on their body for controlling the robotic arm to reach three target positions in the robot workspace. Each task was repeated 3 times for each of the three inverse kinematic approaches (i.e. DLS, EP, AJ).

Before starting the experiments, the subjects were instructed to perform calibration movements required to reconstruct arm kinematics (see [21] for further details) and to be in standing position (see Fig. 1) for few seconds. Then he/she moved the arm to a comfortable configuration (i.e. with the upper arm aligned with the trunk, the elbow rotated roughly at 90 degrees and the hand palm pointing toward the chest) before starting the task, in order to let the robot move to this starting configuration. The data acquired from the IMUs were used for moving the robot arm from its initial pose to the human corresponding pose by means of a fifth order polynomial interpolation on each joint value. Then the subject started to control the robot movements for reaching the target position. During the task execution, the participants were located behind the robot in order to continuously see the robot motion.

III Results

The teleoperated controls based on the previously described inverse kinematics algorithms were validated in simulation and on a real robotic arm, i.e. the KUKA LWR4+. In simulation, the inverse kinematics error was computed, obtaining values lower than one millimeter for the position and one degree for the orientation. These preliminary results showed the effectiveness of algorithm implementation.

Then, the approaches were validated on the KUKA LWR (Fig. 3). In order to achieve the best performance, each algorithm's gain value was empirically estimated. Performance parameters were defined as (i) the error between the human hand and the robot end-effector pose and (ii) positional error between the robot end-effector and the three targets.

For the sake of brevity, only the results obtained by one subject performing one task are shown. In particular, the error between human hand and robot end-effector position and the *SO*3 norm of the orientation error between the human hand and the robot end-effector using the three inverse kinematics approaches are shown in Figs. 4 and 5, respectively.

The mean estimated performance value for each recruited subject are shown in table I. Mean value were computed on the whole task trajectory. Additionally the positional error between end-effector and fixed target were reported as general quality indicator of task performance.

As evident from Figs. 4 and 5, comparable performance were obtained for the three methods, as revealed also in table I.

The error between hand and end-effector pose deeply decreasing when the target is reached and a static pose is maintained, as we can see in the last column of table I. Concerning the anthropomorphic indicators, both the swivel angle error measure and the error between the human and the robot elbows positions seem to assume high value. Nevertheless, the reason is the implementation of moderate anthropomorphic constraints instead of hard constraints, in order to achieve human-like behaviour on the slave side, preserving high accuracy on the end-effector pose (and the target reaching). The main performance dissimilarity between algorithms consists in the target reaching. Indeed, except for subject 2, the EP method showed the lowest error between the end-effector and the target positions, suggesting its easer use with respect to the other methods. On the other hand, the EP method results to have the highest error in static poses. Probably the selected gain values make this method lower accurate than the others, but overall more intuitive for subjects. A new selection of the gain values could improve the accuracy of the algorithm, preserving his usability.

It is worth noticing that the proposed approach, especially the initial configuration, is based on a robot to human joint correspondence. This implies that the robot should be installed with the base on the wall, if the subject is standing (or seated). However, we performed the task on a robot pre-installed on a table, implying some difficulties for the subjects in accomplishing the task and, therefore, decreasing their performance.

IV   Conclusions

In this paper we proposed a teleoperated approach for an anthropomorphic manipulator using IMUs on the master side and involving anthropomorphic criteria to obtain human-like behaviours on the slave side. Using human arm movements as input, and implementing anthropomorphism criteria on robot movements allowed the user to control the robotic platform more easily and intuitively than traditional master interfaces. A fingertip mapping method based on forward-inverse kinematics computed on the master and slave sides was adopted. Three different inverse kinematics algorithms (DLS, EP, AJ) were implemented on the slave side, two of these involving anthropomorphic constrains in the joint space, based on the robot and human elbows position measure. Four Xsens MTws sensors and a KUKA LWR 4+ robot arm were used to experimentally validate the teleoperated approach. Four subjects were recruited and asked to perform three reaching tasks. The implemented

algorithms resulted to have comparable performance in terms of error between hand and end-effector pose. For instance, for subject 1, we have the following mean values:

- DLS: 12.34 ± 8.94 mm and 3.81 ± 2.76 deg

- EP: 15.64 ± 8.33 mm and 4.07 ± 2.74 deg

- JA: 11.67 ± 9.02 mm and 2.79 ± 2.12 deg

Nevertheless, the EP method showed the lower position error for targets reaching, suggesting its easier use by the subjects with respect to the other methods. On the contrary, the EP method showed also the higher static error during the last trajectory's second. Therefore in the future new gain values could be selected in order to improve the EP performance, preserving its usability. Future works will be addressed to enhance the system performance by adjusting the algorithm gain values and to extend the study on a greater number of subjects. Questionnaires for assessing system usability will be also submitted to the subjects.

Acknowledgments

References

[1]. Siciliano, Bruno; Khatib, Oussama, editors. Springer handbook of robotics. Springer; 2016.

[2]. url: http://www.davincisurgery.com

[3]. Cui, Jianhong; , et al. A review of teleoperation system control. Proceedings of the Florida Conference on Recent Advances in Robotics; Boca Raton, FL. Florida Atlantic University; 2003.

[4]. Wang, Yuting. Closed-form inverse kinematic solution for anthropomorphic motion in redundant robot arms. Diss. Arizona State University; 2013.

[5]. Liarokapis, Minas; , et al. Deriving Humanlike Arm Hand System Poses. Journal of Mechanisms and Robotics. 2017; 9(1)

[6]. Artemiadis, Panagiotis K; Katsiaris, Pantelis T; Kyriakopoulos, Kostas J. A biomimetic approach to inverse kinematics for a redundant robot arm. Autonomous Robots. 2010; 29(3):293–308.

[7]. Hollerbach, John M; Jacobsen, Stephen C. Anthropomorphic robots and human interactions. Proc of the 1st International Symposium on Humanoid Robots; 1996.

[8]. Cordella, Francesca; Zollo, Loredana; Guglielmelli, Eugenio. A RGB-D Camera-Based Approach for Robot Arm-Hand Teleoperated Control. 20th IMEKO TC-4 International Symposium Measurement of Electrical Quantities, Special Session on Transducers for robot autonomous navigation;

[9]. Lauretti, Clemente; Cordelladi Luzio, Scotto; Sacchetti, Saccucci; Davalli, et al. Comparative performance analysis of m-imu/emg and voice user interfaces for assistive robots. 15th IEEE International Conference on Rehabilitation Robotics; 2017.

[10]. Liarokapis, Minas V; Artemiadis, Panagiotis K; Kyriakopoulos, Kostas J. Functional anthropomorphism for human to robot motion mapping. RO-MAN, 2012 IEEE; IEEE; 2012.

[11]. Liarokapis, Minas V, , et al. Directions, methods and metrics for mapping human to robot motion with functional anthropomorphism: A reviewTech Rep. School of Mechanical Engineering, National Technical University of Athens; 2013.

[12]. Rohling, Robert. Optimized fingertip mapping and hand modeling for telemanipulation. Masters thesis, McGill University; 1993.

[13]. Artemiadis, Panagiotis K; Katsiaris, Pantelis T; Kyriakopoulos, Kostas J. A biomimetic approach to inverse kinematics for a redundant robot arm. Autonomous Robots. 2010; 29(3):293–308.

[14]. Papaleo, Eugenia; , et al. Upper-limb kinematic reconstruction during stroke robot-aided therapy. Medical & biological engineering & computing. 2015; 53(9):815–828. [PubMed: 25861746]

[15]. Koenemann, Jonas; Burget, Felix; Bennewitz, Maren. Real-time imitation of human whole-body motions by humanoids. Robotics and Automation (ICRA), 2014 IEEE International Conference on. IEEE; 2014.

[16]. Asfour, Tamim; Dillmann, Rdiger. Human-like motion of a humanoid robot arm based on a closed-form solution of the inverse kinematics problem. Intelligent Robots and Systems, 2003. (IROS 2003). Proceedings. 2003 IEEE/RSJ International Conference on. Vol. 2; IEEE; 2003.

[17]. Lauretti, Clemente; CordellaGuglielmelliZollo. Learning by Demonstration for planning activities of daily living in rehabilitation and assistive robotics. Robotics and Automation Letters. 2017

[18]. Bischoff, Rainer; , et al. The KUKA-DLR Lightweight Robot arm- a new reference platform for robotics research and manufacturing. Robotics (ISR), 2010 41st international symposium on and 2010 6th German conference on robotics (ROBOTIK); VDE; 2010.

[19]. Xsens Technologies. http://www.xsens.com

[20]. Bellusci, G, Dijkstra, F, Slycke, P. Xsens MTw: Miniature wireless inertial motion tracker for highly accurate 3D kinematic applications. Xsens Technologies; 2013.

[21]. Ricci, Luca; , et al. A new calibration methodology for thorax and upper limbs motion capture in children using magneto and inertial sensors. Sensors. 2014; 14(1):1057–1072. [PubMed: 24412901]
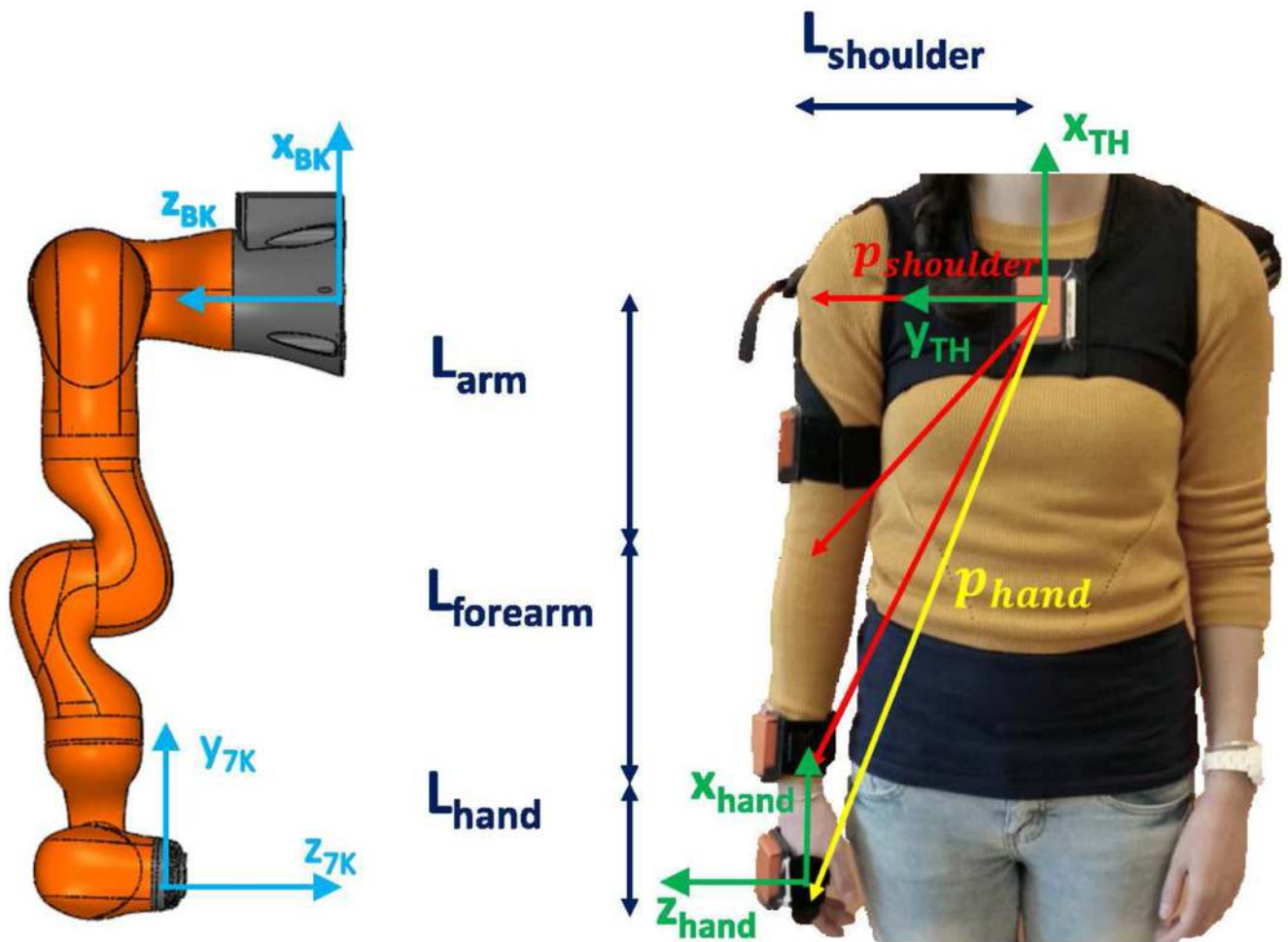
Fig. 1.
Initial configuration of the human and robotic arms. On the left side the KUKA initial configuration with its base and end-effector reference frames is shown. On the right side the human configuration with IMUs placed on thorax, arm, forearm and hand link using click-in body straps is shown. Human thorax and hand reference frames are outlined. Hand position p_{hand} is computed as vectorial sum of each arm joint vector.
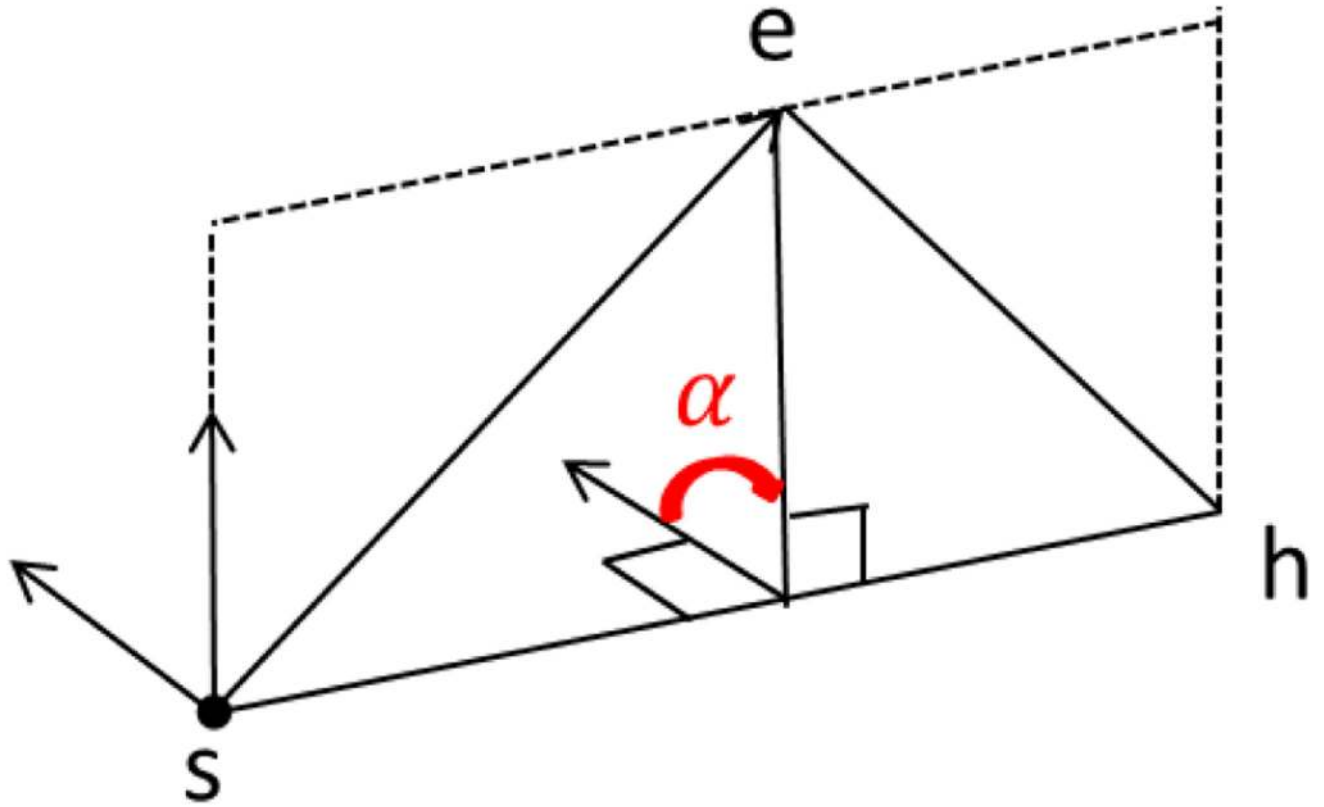
Fig. 2.
Swivel angle (α) representing the elbow position (e) for fixed shoulder (s) and hand (h) positions.
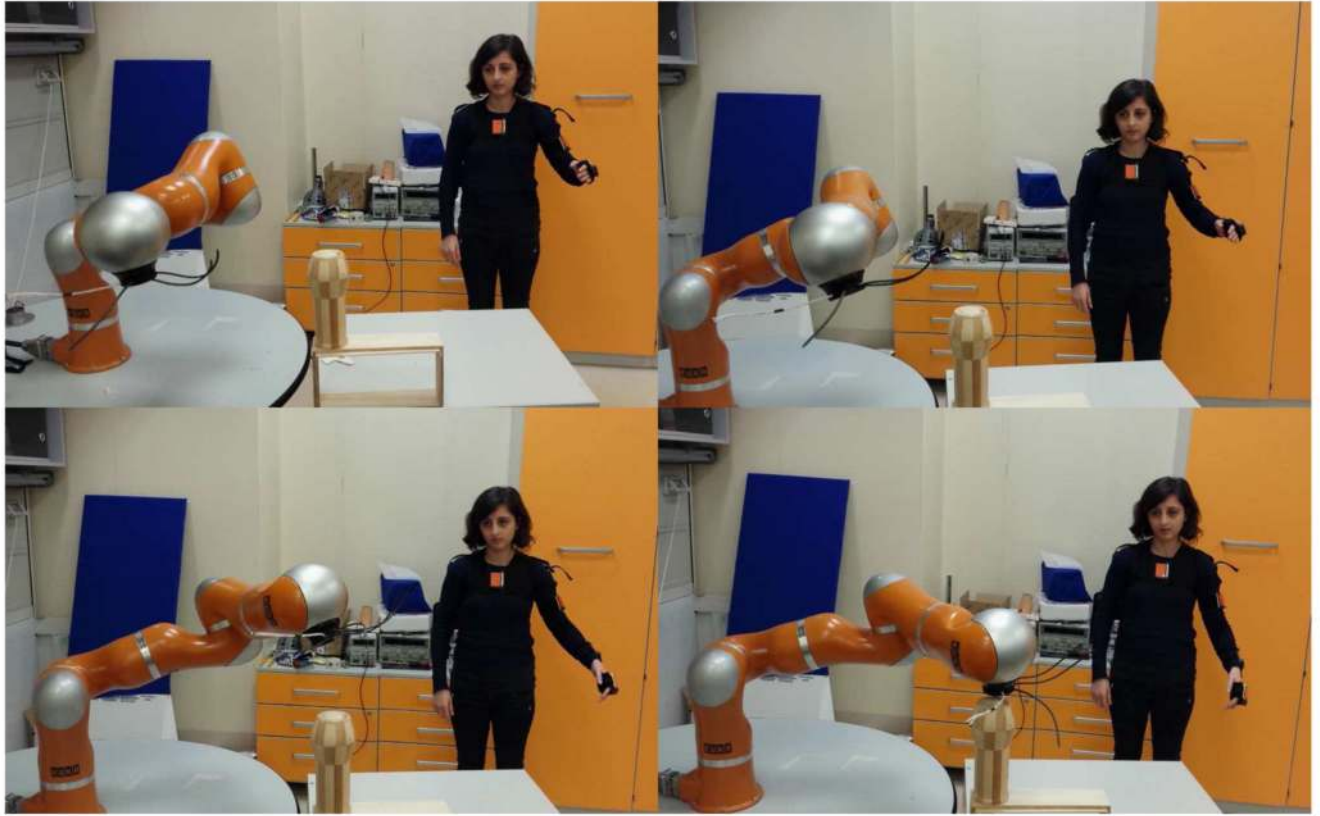
Fig. 3.
Experimental validation on the KUKA LWR4+. Four frames of the reaching task performed by Subject 1 are shown.
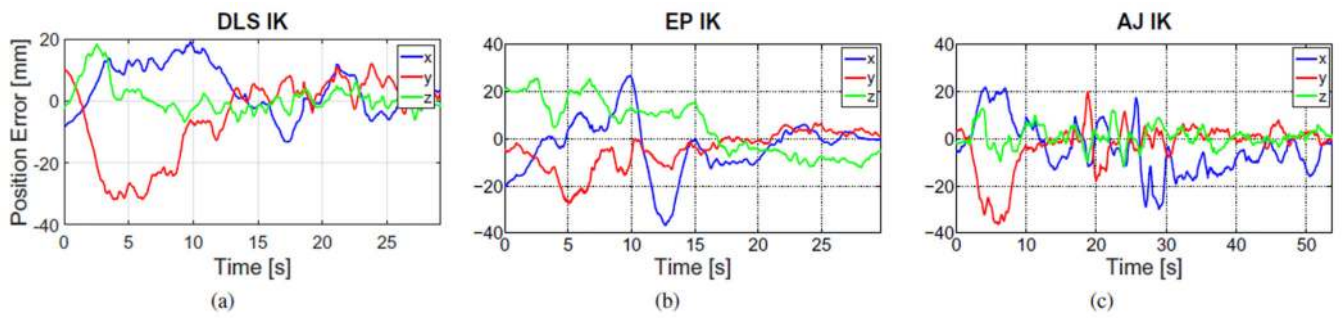
Fig. 4.
Error between the human hand and the robot end-effector position using the a) DLS, b) EP and c) AJ algorithm. The values were estimated during the reaching task performed by subject 1.
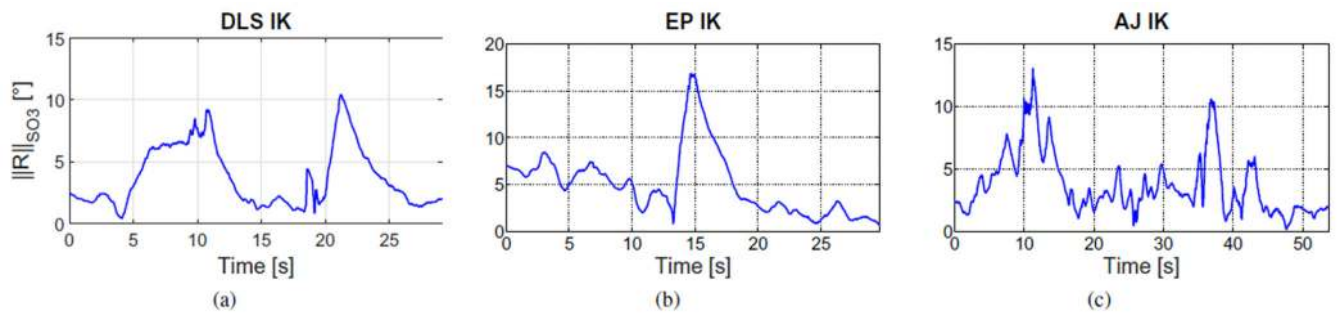
Fig. 5.

*SO*3 norm of the orientation error between the human hand and the robot end-effector using the a) DLS, b) EP and c) AJ algorithm. The values were estimated during the reaching task performed by subject 1.
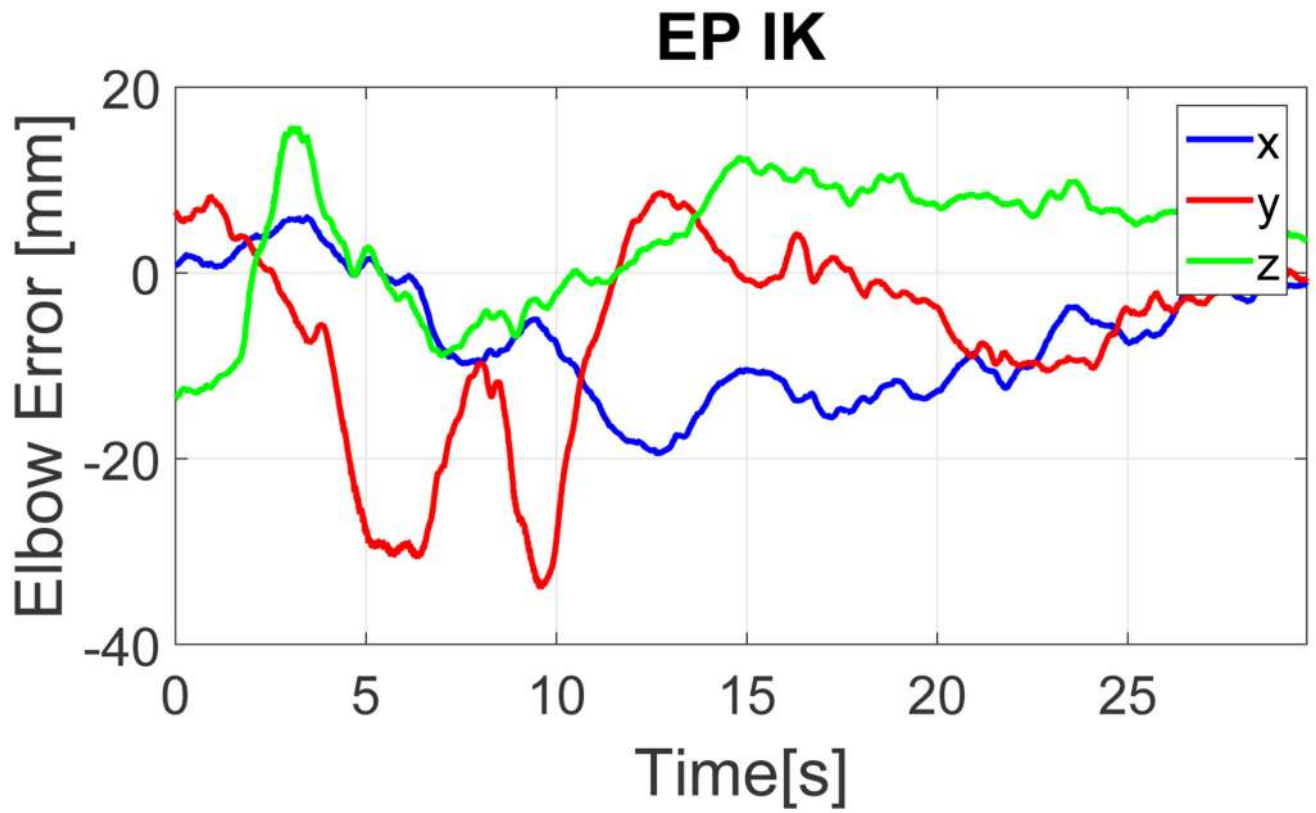
Fig. 6.
Error between human and robot elbow position using the EP algorithm. The values were estimated during the reaching task performed by subject 1.
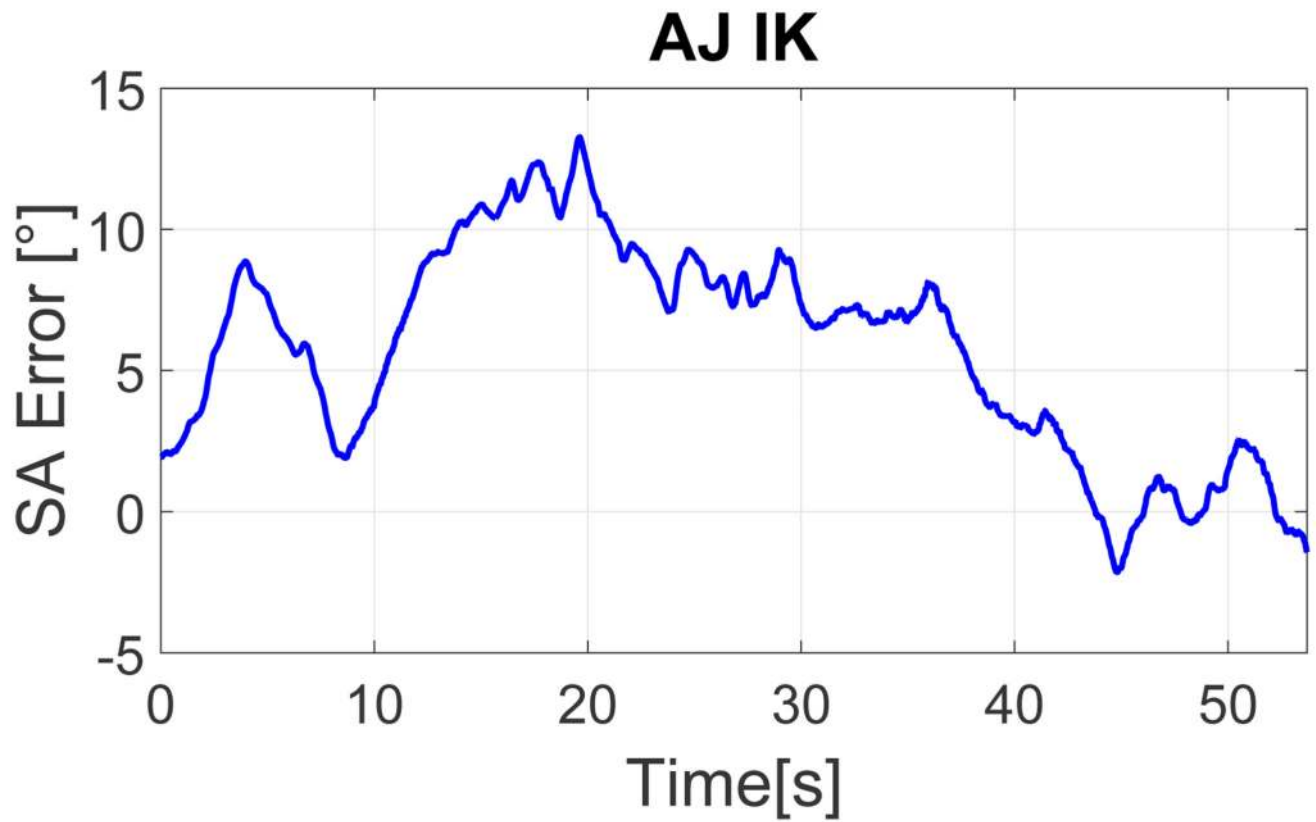
Fig. 7.
Error between human hand and robot swivel angle using the AJ algorithm. The values were estimated during the reaching task performed by subject 1.

Table I

Experimental results: (i)$\|PosErr\|$ is the mean norm error between the human hand and the end-effector position during the whole trajectories; (ii)$\|R\|_{SO3}$ is the mean $SO3$ norm of the rotation matrix between the hand and end-effector in the whole trajectories; (iii)$\|ElbowPosErr\|$ is the mean norm positional error between human and robot elbow joints during the whole trajectories; (iv) SA Error is the mean error value between human and robot swivel angle; (v)$\|TErr\|$ is the mean norm positional error reaching fixed targets; (vi)$\|SErr\|$ is the static position and orientation error (i.e. $\|PosErr\|$ and $\|R\|_{SO3}$ values for the last trajectory second). Clearly (iii) is computed only for EP method and (iv) only for AJ method.

Sub	Algorithm	$\|PosErr\|$[mm]	$\|R\|_{SO3}$[deg]	$\|ElbowPosErr\|$[mm]	SA Error [deg]	$\|TErr\|$ [mm]	$\|SErr\|$ [mm] [deg]
1	DLS	12.34±8.94	3.81±2.76			32.15	2.49±0.55 0.89±0.09
	EP	15.64±8.33	4.07±2.74	134.33±208.36		24.07	7.28±0.73 1.57±0.17
	AJ	11.67±9.02	2.79±2.12		3.38±2.39	71.58	4.32±0.74 1.38±0.10
2	DLS	9.79±8.30	3.20±2.35			20.79	3.77±0.43 1.80±0.07
	EP	13.05±10.20	3.80±1.94	32.42±34.65		22.88	17.24±1.06 2.28±0.06
	AJ	10.21±8.12	3.91±2.84		2.99±2.18	19.99	4.2±0.70 1.23±0.12
3	DLS	12.37±9.55	4.73±2.85			48.50	6.43±0.88 2.03±0.26
	EP	13.89±12.09	6.58±3.82	140.08±212.02		28.21	23.94±3.61 5.84±0.84
	AJ	13.92±11.95	5.91±2.61		3.74±4.29	39.90	12.33±1.73 3.69±0.45
4	DLS	13.94±12.68	8.33±4.17			31.56	15.84±1.84 5.17±0.56
	EP	13.69±11.40	11.47±6.34	132.78±208.16		25.29	21.74±4.43 6.14±0.56
	AJ	11.45±8.64	2.15±3.29		3.61±8.74	35.12	7.11±1.10 2.69±0.39